

Supplementary Material

Mathematically, the coordinate transformation describing the rigid-body motion can be expressed as:

$$\mathbf{r}' = T_{\Theta}(\mathbf{r}) = \begin{bmatrix} 1 & 0 & 0 \\ 0 & \cos(\theta_x) & -\sin(\theta_x) \\ 0 & \sin(\theta_x) & \cos(\theta_x) \end{bmatrix} \begin{bmatrix} \cos(\theta_y) & 0 & \sin(\theta_y) \\ 0 & 1 & 0 \\ -\sin(\theta_y) & 0 & \cos(\theta_y) \end{bmatrix} \begin{bmatrix} \cos(\theta_z) & -\sin(\theta_z) & 0 \\ \sin(\theta_z) & \cos(\theta_z) & 0 \\ 0 & 0 & 1 \end{bmatrix} \begin{bmatrix} x \\ y \\ z \end{bmatrix} + \begin{bmatrix} \eta_x \\ \eta_y \\ \eta_z \end{bmatrix} \quad (1)$$

where $\mathbf{r} = [x, y, z]^T$ and \mathbf{r}' denote the spatial coordinates before and after the transformation, $\Theta = \{\theta_x, \theta_y, \theta_z, \eta_x, \eta_y, \eta_z\}$ contains the rotation and translation motion parameters. To perform sensitivity alignment, the motion parameters are estimated by solving the following least square problem:

$$\hat{\Theta} = \underset{\Theta}{\operatorname{argmin}} \|S(T_{\Theta}(r)) - S_{ref}\|_2^2 \quad (2)$$

where S and S_{ref} denote the current and the reference sensitivity maps. Given the determined parameters, the aligned sensitivity is calculated by $S' = S(T_{\Theta}(r))$ using cubic interpolation. The estimated rotation and translation parameters from the GRE scans are shown in Fig. S1. As can be seen, the largest rotation occurs about the x-axis (pitch rotation), which is sensitive to both the head position and axial slices selection. The largest translation occurs along the z-axis (head foot direction).

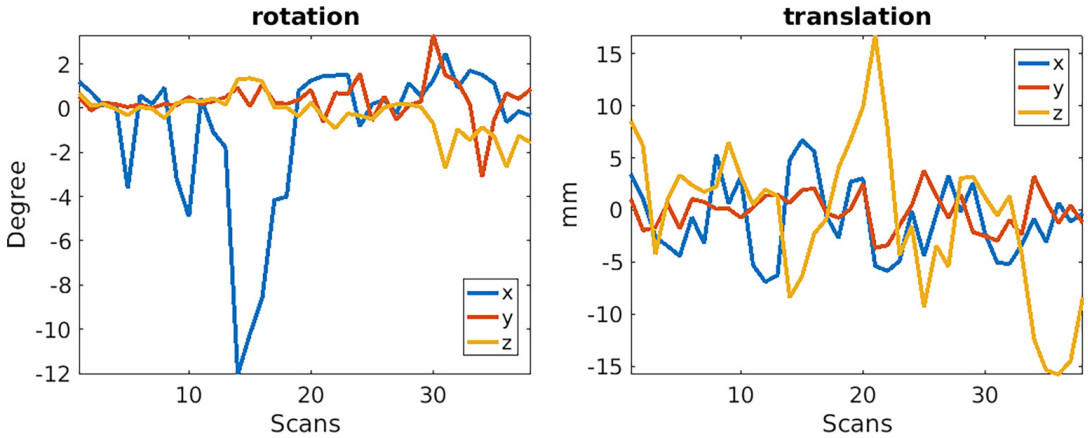


FIGURE S1 Estimated rotation and translation parameters of the sensitivity functions from the different GRE scans with respect to the first scan. The largest rotation occurs about the x-axis (pitch rotation), which is sensitive to both the head position and axial slices selection. The largest translation occurs along the z-axis (head foot direction).

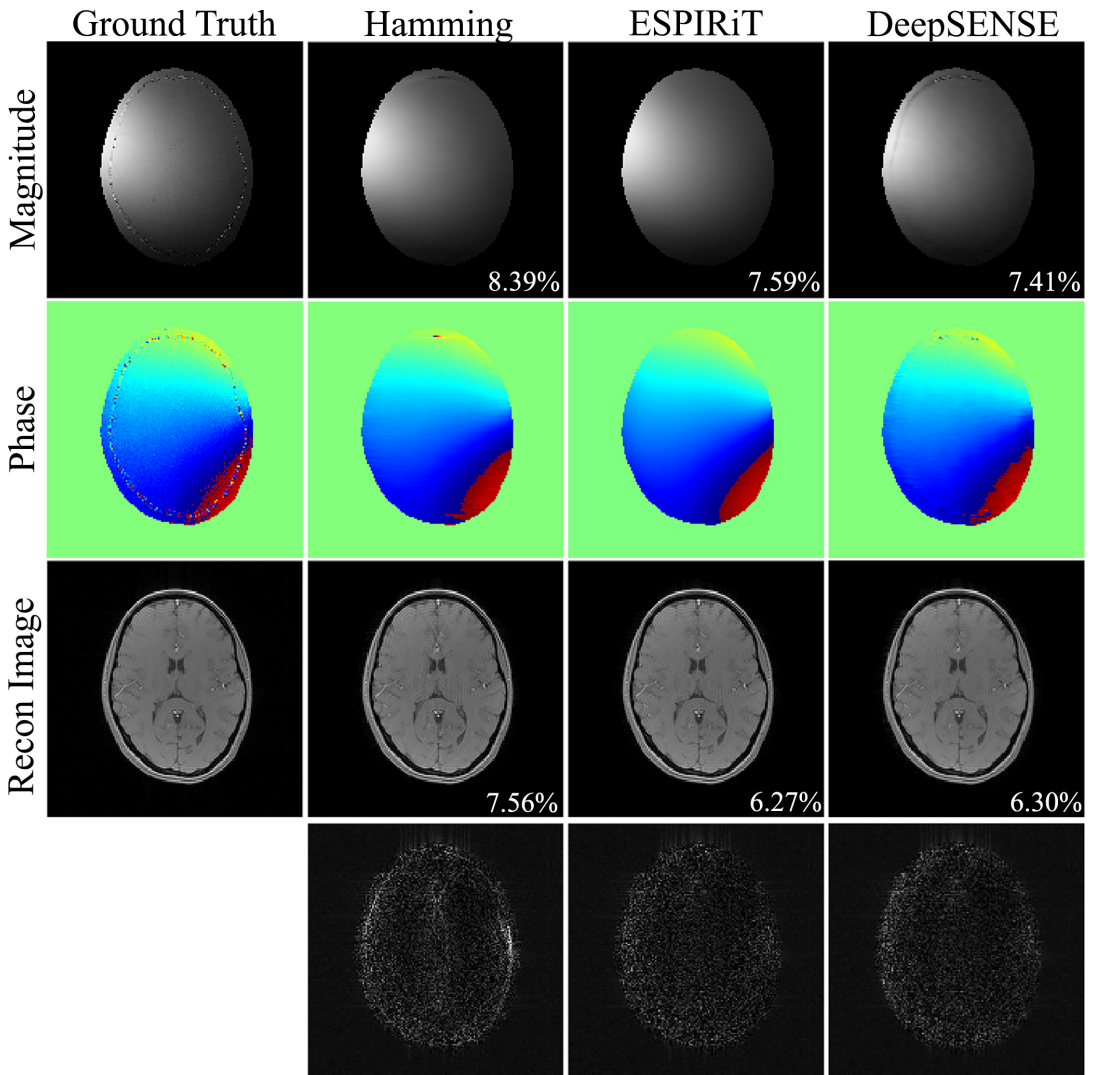


FIGURE S2 The sensitivity maps estimated using 24 ACS lines and the subsequent iterative SENSE reconstructions at R=4 of a GRE testing dataset. RMSEs of the sensitivity maps and SENSE reconstructions are shown in the magnitude image.

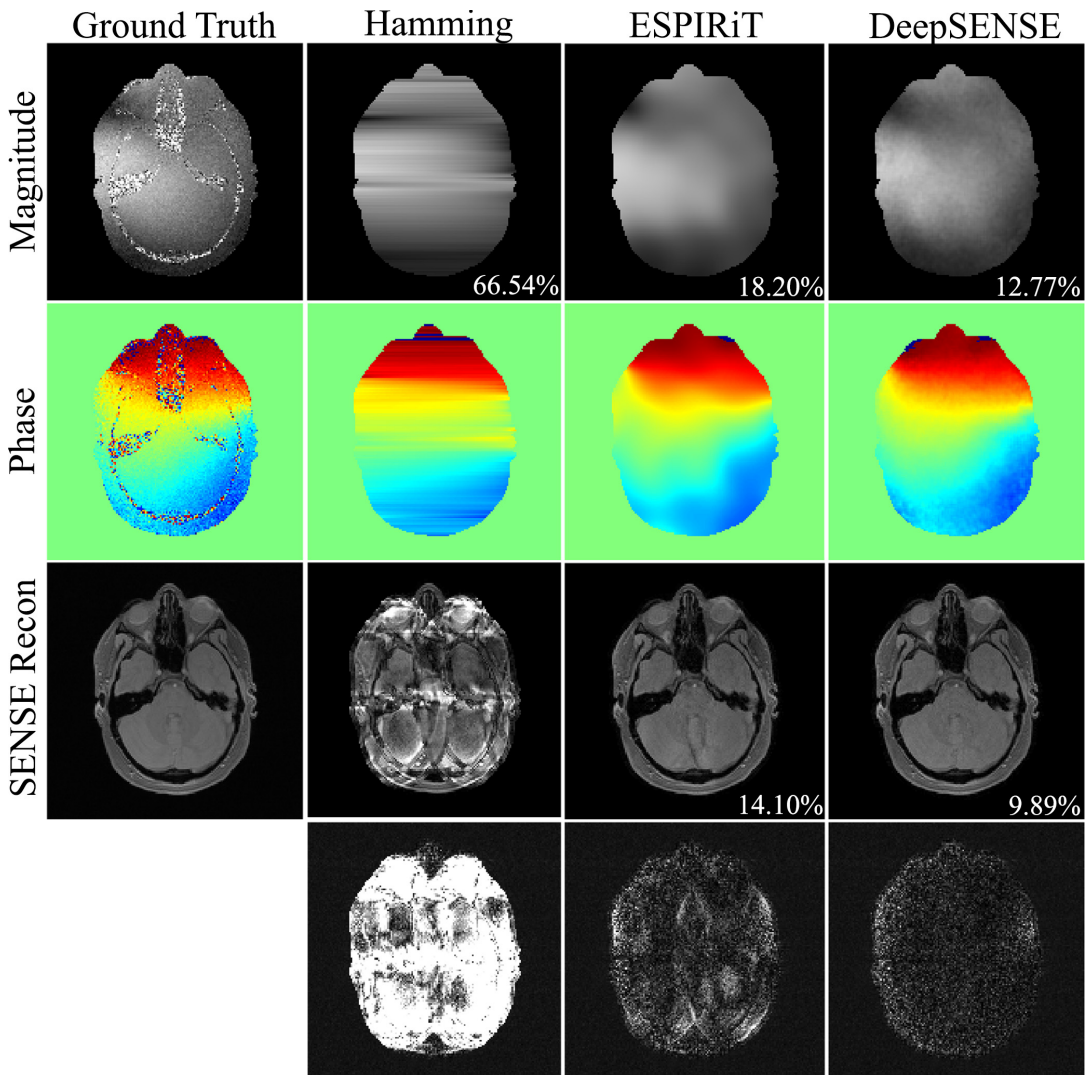


FIGURE S3 The sensitivity maps estimated using 4 ACS lines and the subsequent iterative SENSE reconstructions at R=4 of a bottom brain slice with air-tissue interface. RMSEs of the sensitivity maps and SENSE reconstructions are shown in the magnitude image.

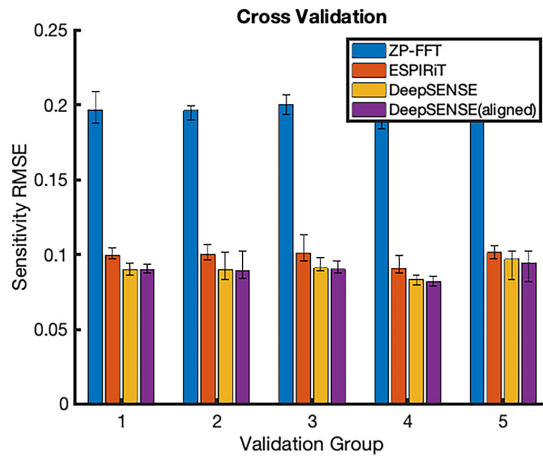


FIGURE S4 Sensitivity RMSEs from the 5-fold cross validation estimated using 8 ACS lines. Results showed that the learning-based method was able to improve the sensitivity estimation to a similar level (approximately a mean RMSE of 7.8%) for all the validation groups with a relatively small set of training data, further validating our hypothesis that the coil sensitivity between scans reside on a low-dimensional manifold. Note that coil alignment improved the sensitivity estimation for group 4 and 5 (possibly larger spatial misalignment), but may not be necessarily required in the case of small spatial misalignment (group 1-3), since the deep CNN should be able to handle certain extent of geometric variation due to its powerful representation capability.

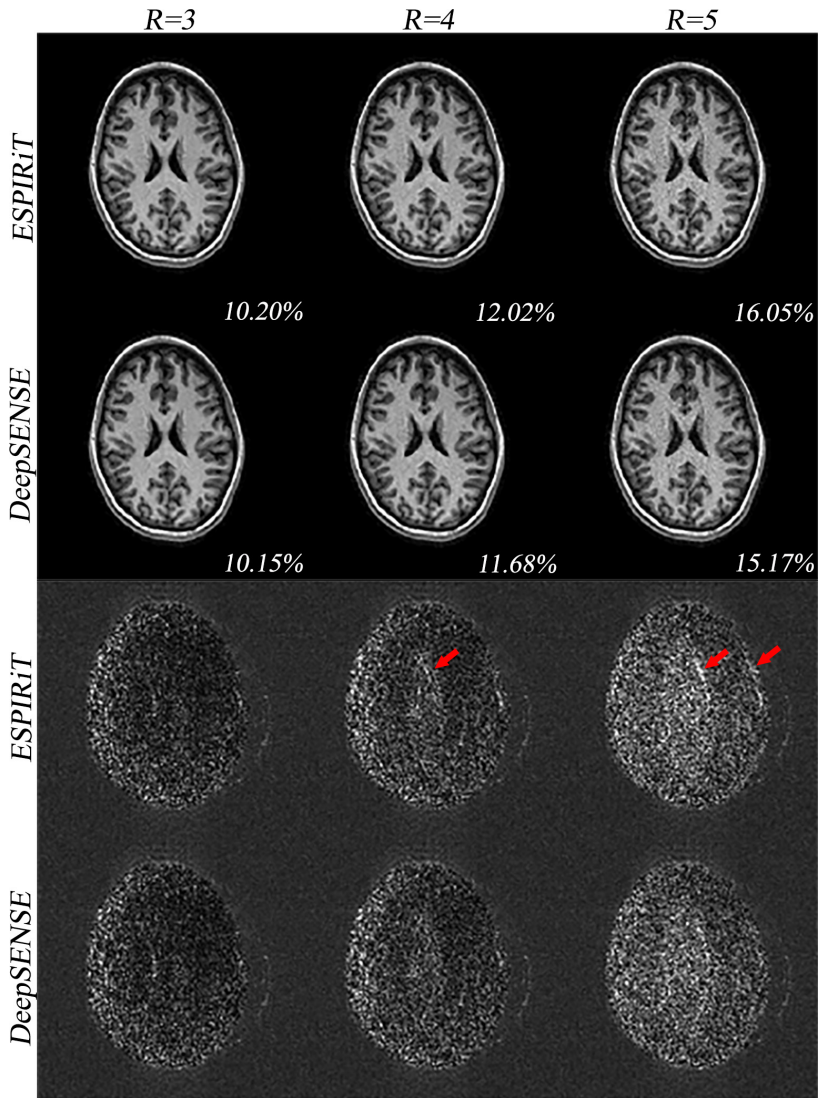


FIGURE S5 Iterative SENSE reconstructions of the MPRAGE dataset with uniform undersampling in the outer k-space at various reduction factors (i.e., $R = 3, 4, 5$). The ESPiRiT and the proposed DeepSENSE methods were used for sensitivity estimation from 8 ACS lines. Error maps were scaled by 5 folds for better visualization. Although the proposed model was trained on the GRE dataset, it still enables improved sensitivity estimation manifested by the reduced aliasing and noise amplification in the SENSE reconstruction.